(Philodinida, Philodinidae), *Habrotrocha constricta* (Philodinida, Habrotrochidae), and *Adineta vaga* (Adinetida, Adinetidae). Monogononta: *Brachionus plicatilis* strains AUS and RUS, *Brachionus calyciflorus* (Ploima, Brachionidae), *Eosphora ehrenbergi* (Ploima, Notommatidae), and *Sinantherina socialis* (Flosculariacea, Flosculariidae). Seisonida: *Seison nebaliae*. Acanthocephala: *Moniliformis moniliformis*. Attribution and provenance are available at *Science* Online at www.sciencemag.org/feature/data/1050064.shl. Bdelloids, *B. calyciflorus*, and both strains of *B. plicatilis* were kept in large (10^4 to 10^5) cultures grown from single eggs or single individuals after 10 serial passages through sterile water in microtitre wells. Culture conditions and DNA extraction procedures are described elsewhere (*21*, *36*). DNA was extracted from a single colony of *S. socialis* and from single field collections of *E. ehrenbergi* and *S. nebaliae* (*10*). Primer sequences and PCR protocols are available from the authors or at *Science* Online at www.sciencemag.org/feature/data/1050064.shl. Each sequence found was represented in at least five cloned amplicons from at least two amplifications, except *hsp82* copy 2 of *P. roseola*, which was found only in the cosmid library. Occasionally, a single PCR clone differed from a set of otherwise identical clones at one or two sites, which could be attributed to an error rate of about 0.0003 per nucleotide, similar to the error rate reported in other PCR cloning experiments (*37*, *38*). The *hsp82* region in 36 phage lambda clones and 25 cosmid clones selected from genomic libraries of *P. roseola* was also sequenced.

31. W.-H. Li, *J. Mol. Evol.* **36**, 96 (1993).
32. D. B. Mark Welch, thesis, Harvard University, Cambridge, MA (1999).
33. T. Mukai, S. I. Chigusa, L. E. Mettler, J. F. Crow, *Genetics* **72**, 335 (1972).
34. H.-W. Deng and M. Lynch, *Genetics* **144**, 349 (1996).
35. S. A. Shabalina, L. Y. Yampolsky, A. S. Kondrashov, *Proc. Natl. Acad. Sci. U.S.A.* **94**, 13034 (1997).
36. J. L. Mark Welch and M. Meselson, *Hydrobiologia* **387/388**, 403 (1998).
37. A. M. Dunning, P. Talmud, S. E. Humphries, *Nucleic Acids Res.* **16**, 10393 (1988).
38. P. D. Ennis, J. Zemmour, R. D. Salter, P. Parham, *Proc. Natl. Acad. Sci. U.S.A.* **87**, 2833 (1990).
39. M. L. Goddemeier and G. Feix, *Gene* **174**, 111 (1996).
40. W. Gilbert, M. Marchionni, N. G. McKnight, *Cell* **46**, 151 (1986).
41. N. Inomata, H. Tachida, T. Yamazaki, *Mol. Biol. Evol.* **14**, 942 (1997).
42. H. M. Robertson, *Genome Res.* **8**, 449 (1998).
43. DNA sequences were aligned (*10*) and analyzed with the Wisconsin Package 10.0 (Genetics Computer Group) and the PHYLIP v3.57 package of J. Felsenstein. Uncorrected difference at fourfold degenerate sites (D4) was determined from pair-wise comparisons with DIVERGE. Phylogenetic analyses used all codon third positions belonging to conserved fourfold or threefold degenerate codon classes plus third positions in those few cases where a codon in a single bdelloid sequence differed from a fourfold or threefold degenerate class by no more than a single substitution. Distances for neighbor-joining were adjusted for multiple mutations with the Kimura two-parameter model with rates following a gamma distribution with a coefficient of variance (CV) of 1.41 estimated for both genes from the maximum likelihood algorithm in PAUP*. The same tree topologies, with similar bootstrap support, are found with a range of CV.

44. We thank E. Lemyre and D. Kunimoto for assistance in early stages of this work; I. Arkhipova, J. Crow, G. Giribet, J. Mark Welch, B. Normark, and F. Stahl for critically reading the manuscript; and the Eukaryotic Genetics Program of the NSF for consistent support. D.M.W. was supported by an NSF Graduate Research Grant. This article is dedicated to G. Evelyn Hutchinson. GenBank accession numbers for the reported sequences are AF143849 to AF143858 and AF249985 to AF250004.

3 March 2000; accepted 28 March 2000

Rocks from the Mantle Transition Zone: Majorite-Bearing Xenoliths from Malaita, Southwest Pacific

Kenneth D. Collerson,[1]* Sarath Hapugoda,[1] Balz S. Kamber,[1] Quentin Williams[2]

Rocks containing high-pressure mineral assemblages derived from the mantle transition zone between depths of about 400 and 670 kilometers occur as xenoliths and megacrysts on the island of Malaita in the southwest Pacific on the Ontong Java Plateau. Observed ultrahigh pressure mineral chemistries include majorite, calcium- and magnesium-perovskite, aluminous silicate phases, and microdiamond. Based on an empirical barometer, majoritic garnets in these xenoliths record pressures of up to 22 gigapascal. The occurrence of material with perovskite chemistry and several enigmatic aluminous phases indicates pressures of up to 27 gigapascal. Samples were brought to the surface at about 34 million years ago by potassic ultramafic magmas, which evidently originated in the lower mantle.

Xenoliths, the main direct source of information about mantle mineralogy, are predominantly derived from the top of the upper mantle, from depths of ~150 to 200 km (*1*, *2*), although some have been reported from depths of ~400 km (*3*, *4*). Mineral inclusions in diamond are generally interpreted to yield a record of phase relations at depths of 150 to 200 km, equivalent to pressures of ~5.5 to 7 GPa (*5*, *6*). Extremely rare single-mineral inclusions of ferropericlase, Mg-Si perovskite, Ca-Si perovskite, and magnesiowustite have recently been discovered in diamond derived from the lower mantle (*7*). Most deep xenoliths and diamonds are transported in kimberlites and lamproites that intrude continental lithosphere (*1*, *8*). Here, we describe an extensive suite of garnetite and rare garnet peridotite xenoliths that contain majoritic and other ultrahigh pressure mantle assemblages, indicating that these rocks sample the mantle transition zone in an oceanic environment.

Geology and Locality

The xenoliths and macrocrysts occur in ~34 Ma (million years ago) alnöite pipes and sills (*9*), which cut Cretaceous Ontong Java Plateau basalts, Miocene limestones, and mudstones on the island of Malaita, southwest Pacific (Fig. 1). The oceanic Ontong Java Plateau covers an area of 1.28×10^6 km^2 to the northeast of the Solomon Island archipelago and Bougainville Island (Fig. 1) and is one of the largest plume-generated intraplate igneous provinces preserved on the planet. Volcanic activity on the Ontong Java Plateau commenced at ~122 Ma, and a second major pulse of magmatism occurred at 90 Ma (*10*). At this time, the Ontong Java Plateau was located several thousand km farther east in the central Pacific Ocean (*11*). Igneous rocks on Malaita have a plume origin, distinct from the arc-generated islands in the Solomon Archipelago (*10*).

Seismic reflection profiles show that Ontong Java Plateau basalts are cut by numerous distinctive plug-like bodies that vary in diameter up to ~2.5 km (*11*) and may be kimberlite pipes (*12*). Alnöitic magmatism at ~34 Ma occurred before collision of Malaita with the Indo-Australian plate ~10 Ma (*13*), and before initiation of geologically unrelated Solomon Islands arc magmatism (*12*, *14*).

We obtained mantle xenoliths and garnet macrocrysts from stream gravels in several drainage systems from the north central and eastern parts of the island (*15*), where a number of pipes have been mapped. The studied ultramafic xenoliths are ovoid in shape and range in diameter from <1 to 30 cm. Compositions include spinel lherzolite, pyroxenite intergrowths, spinel bearing eclogite, and rare garnet lherzolite. The macrocrysts suite includes pyrope, subcalcic diopside, augite, orthopyroxene (bronzite), ilmenite, clinopyoxene-ilmenite intergrowths, phlogopite, olivine, and zircon (*14*, *16*, *17*). Many of the macrocrysts exhibit a distinctive surficial polish that is interpreted to have been caused by abrasion during turbulent magmatic emplacement. Garnet macrocrysts are typically elongate and range in size from ~1 cm by 0.5 cm by 0.5 cm to larger than 20 cm by 10 cm by 10 cm. Except for olivine, all of the other macrocrystal phases are extremely fresh.

---

[1] Department of Earth Sciences, The University of Queensland, Brisbane, Qld 4072, Australia. [2] Department of Earth Sciences, University of California Santa Cruz, Santa Cruz, CA 95064, USA.

*To whom correspondence should be addressed. E-mail: k.collerson@mailbox.uq.edu.au

Garnet and Majorite

We obtained more than 600 analyses (*18*) of garnets in 19 samples. Results are given in Tables 1 through 3 and in Web table 1 (*18*). Most of the garnets (~99%) are derived from eclogite protoliths (E-type). They are pyrope-rich with Mg/(Mg+Fe) = 0.69 to 0.82 and Cr_2O_3 < 0.5 weight percent (wt %). Rare (~1%) peridotite derived garnets (P-type) have Mg/(Mg+Fe) = 0.82 to 0.92 and Cr_2O_3 = 1.0 to 2.8 wt % (Table 1). The TiO_2 and Na_2O contents in P- and E-type pyropes are <0.2 and 0.1 wt % and 0.4 to 0.7 wt %, respectively, and some majoritic garnets contain 3.2 wt % TiO_2 and 4.3 wt % Na_2O (Tables 1 and 2).

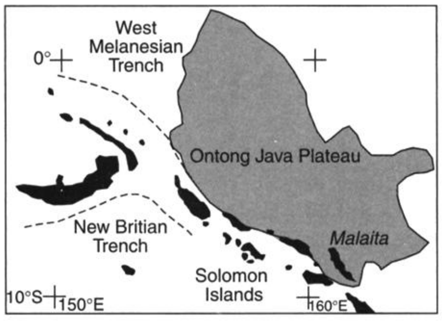

Fig. 1. Map showing the location of Malaita on the Ontong Java Plateau. Igneous rocks on Malaita have a mantle plume origin, distinct from the arc generated islands in the Solomon Archipelago (*10*). Collision of Malaita with the Indo-Australian plate occurred ~10 Ma (*13*), before initiation of Solomon Islands arc magmatism (*12, 14*).

Both E- and P-type garnets show an extreme range of covariation between Si and Al+Cr (Fig. 2A). They show excellent stoichiometry and define a well-correlated trend between pyrope, with $Si^{4+} = 3$ per formula unit (pfu; based on 12 oxygens) and Al+Cr = 2 pfu, and ideal clinopyroxene (*19*), with $Si^{4+} = 4$ pfu and Al+Cr = 0 pfu (Fig. 2A). The slope of the combined vector defines continuous solid solution in majoritic compositions from 3.2 Si^{4+} pfu to 3.8 Si^{4+} pfu, which we interpret to reflect the incorporation of Si^{4+} in octahedral coordination in garnet.

An important consideration is whether compositional data can be used to discriminate between majoritic garnet-derived material and simple aluminous pyroxene (such as omphacite). Hypothetical end-member majorite and Al-free clinopyroxene have identical compositions (4 Si^{4+} pfu relative to 12 oxygen atoms), and it would be impossible to distinguish between them based solely on mineral chemistry. This argument is not relevant to the Malaita majorites, as the most silicic compositions have <3.82 Si^{4+} pfu. Data for aluminous pyroxene diamond inclusions compiled from worldwide kimberlite occurrences and representative majorite compositions from Tables 1 and 2 are compared in Fig. 2B. The clinopyroxene data show the expected jadeite substitution vector yielding a slope similar to unity. By contrast, Al and Cr in the majoritic garnets are not balanced by Na and K substitutions. Majorite substitution into garnet mainly involves the M^{2+} cations (Fe, Ca, and Mg) which explains the horizontal vector in Fig. 2B. A further consideration is that the clinopyroxene diamond inclusions, when recalculated to 12 oxygens, have an average Si^{4+} pfu of 3.94 ± 0.08 (Fig. 2C), which is significantly greater than the most silicic majoritic garnet. These clinopyroxenes do not plot on the majorite vector, instead they define a very different, much steeper vector, because Al incorporation

Table 1. Analyses of garnet standard and representative compositions of Malaita garnets and majorites.

Rock type:	Standard		Peridotite				Ecologitic garnetite							
Mineral:	Pyrope		Garnet		Majorite		Garnet		Majorite					
Sample name:	Kakanui pyrope		KC-98-A	KC-98-16	KC-98-16	KC-98-16	KC-99-M3	KC 26	KC M3	KC M2	KC 26	KC-98-19	KC-98-18	KC-99-M5
Remarks or spot identification:	This study (*n* = 9)	Certified value	#128	#31	#10	#24	#62	#18	#131	#138	#23	#118	#78	#240
SiO_2	41.60 ± 0.33	41.98	41.87	42.26	46.53	52.02	41.73	41.48	45.03	47.04	48.56	49.86	51.09	53.29
TiO_2	0.47 ± 0.09	0.44	0.07	0.11	0.36	0.29	0.44	0.70	0.66	0.72	0.72	0.55	0.60	0.27
Al_2O_3	23.73 ± 0.33	23.52	21.80	22.38	12.52	4.23	23.18	22.71	17.91	14.28	11.25	8.15	6.07	3.88
Cr_2O_3	0.00 ± 0.03	0.07	2.65	1.59	1.57	1.07	0.09	0.03	0.24	0.18	0.04	0.00	0.01	0.00
FeO	10.68 ± 0.24	10.99	6.65	8.12	4.67	2.60	11.61	11.20	12.41	11.41	13.53	14.19	12.97	13.55
MnO	0.28 ± 0.05	0.30	0.36	0.38	0.38	0.07	0.32	0.30	0.36	0.33	0.36	0.37	0.42	0.46
MgO	18.51 ± 0.25	18.45	19.61	20.35	14.14	15.68	18.05	17.83	23.29	24.81	23.54	25.38	26.52	27.29
CaO	5.17 ± 0.07	5.01	5.85	3.71	18.06	20.30	4.03	4.71	0.42	1.16	1.97	2.01	1.86	1.92
Na_2O	0.00 ± 0.00	0.02	0.04	0.13	1.09	2.23	0.10	0.09	0.02	0.06	0.17	0.29	0.05	0.13
K_2O	0.00 ± 0.00	0.01	0.02	0.16	0.04	0.11	0.02	0.00	0.00	0.00	0.03	0.00	0.00	0.00
Total	100.4	100.8	98.92	99.19	99.37	98.61	99.58	99.04	100.3	99.99	100.2	100.8	99.59	100.8
Cations per 12 oxygen														
Si^{4+}	2.969 ± 0.008	2.988	3.010	3.022	3.418	3.833	3.007	3.008	3.200	3.345	3.487	3.574	3.680	3.797
Ti^{4+}	0.025 ± 0.005	0.024	0.004	0.006	0.020	0.016	0.024	0.038	0.035	0.038	0.039	0.030	0.032	0.014
Al^{3+}	1.996 ± 0.014	1.972	1.847	1.886	1.084	0.368	1.969	1.940	1.500	1.197	0.952	0.689	0.516	0.326
Cr^{3+}	0.000 ± 0.002	0.004	0.151	0.090	0.091	0.062	0.005	0.002	0.014	0.010	0.002	0.000	0.000	0.000
Fe^{2+}	0.637 ± 0.019	0.654	0.400	0.486	0.287	0.160	0.700	0.679	0.737	0.679	0.812	0.851	0.781	0.807
Mn^{2+}	0.017 ± 0.003	0.018	0.022	0.023	0.023	0.005	0.020	0.018	0.022	0.020	0.022	0.023	0.025	0.028
Mg^{2+}	1.969 ± 0.015	1.957	2.101	2.169	1.548	1.722	1.938	1.927	2.467	2.630	2.519	2.711	2.847	2.898
Ca^{2+}	0.395 ± 0.004	0.382	0.451	0.285	1.422	1.602	0.311	0.366	0.032	0.088	0.151	0.154	0.144	0.146
Na^{+}	0.000 ± 0.001	0.003	0.005	0.019	0.156	0.319	0.014	0.013	0.003	0.009	0.023	0.040	0.007	0.017
K^{+}	0.000 ± 0.000	0.000	0.001	0.014	0.004	0.010	0.002	0.000	0.000	0.000	0.003	0.000	0.000	0.000
Total	8.008 ± 0.008	8.003	7.991	8.000	8.054	8.097	7.990	7.990	8.009	8.016	8.010	8.072	8.033	8.035
Si	2.969 ± 0.008	2.988	3.010	3.022	3.418	3.833	3.007	3.008	3.200	3.345	3.487	3.574	3.680	3.797
Al+Cr	1.996 ± 0.015	1.976	1.997	1.976	1.175	0.430	1.974	1.942	1.513	1.207	0.954	0.689	0.516	0.326
M	3.002	2.996	2.957	2.959	3.413	3.804	2.963	2.984	3.239	3.406	3.506	3.756	3.778	3.869
Pressure estimates (GPa)														
P obtained by Si-barometer			6.4	6.6	14.1	22.0	6.3	6.3	10.0	12.7	15.4	17.1	19.1	21.3
P obtained by Al+Cr-barometer			5.6	5.8	13.1	19.8	5.8	6.1	10.0	12.8	15.1	17.5	19.0	20.8
P average			6.0	6.2	13.6	20.9	6.1	6.2	10.0	12.8	15.2	17.3	19.1	21.0

has evidently no effect on the Si content of pyroxene.

The only pyroxene compositions that could be confused with majoritic garnet are those that experienced tschermak substitution (Al + Al = Si + M^{2+}). Such tschermakitic pyroxenes are either orthorhombic or monoclinic and are thus birefringent. Except for the most siliceous majorite analyses, the Malaita majorite compositions are invariably isotropic. It is significant that the Malaita majorite has the same low Ca content as coexisting metastable pyrope (much lower than the elevated Ca values that are typical of tschermak-rich clinopyroxene). Only Mg-tschermakitic orthopyroxene could be compositionally similar to majoritic garnet. However, the maximum solubility of Al in orthopyroxene is insufficient to explain the full range in composition observed in the Malaita majoritic material (Fig. 2A). Experiments in the pure MgO-Al_2O_3-SiO_2 system have shown that the maximum Al-solubility in orthopyroxene is ~18 mole percent (*20*). This only translates to 3.55 to 3.60 Al ions pfu (per 12 oxygens). Therefore, more than half of the analyses of Malaita majoritic material cannot be explained as aluminous orthopyroxenes. Importantly, in a similar study using natural starting compositions (*21*), Al and Cr contents in orthopyroxenes were lower by ~50% than in corresponding material produced from end-member reagents.

Orthopyroxene and spinel can form as a breakdown product of garnet and olivine in the shallow (<80 km depth) mantle. Such high Al-orthopyroxene is only found in very high-temperature reaction products [i.e., at >1500°C (*20*)] far above the diamond stability field. Orthopyroxenes from within the diamond stability field are more siliceous and have even lower Al contents (Fig. 2C), in agreement with experimental constraints (*20*). The complete absence of olivine in all Malaita garnetites, the presence of phases of exclusively high-pressure origin (i.e., diamond and aluminous silicate phases), and Al content exceeding maximum solubility in orthopyroxene together argue strongly that the phase with majoritic chemistry is indeed majorite.

Majorite is preserved in several habits. E-type majorite occurs in single veins or sets of anastomosing veins up to 300 μm wide in garnet macrocrysts and megacrysts, and also in composite garnetite xenoliths. In some xenoliths, it also occurs randomly distributed as amoeboid areas up to 100 μm in diameter (Fig. 3A). Garnetites consist of garnet (both majoritic and nonmajoritic) and minor spinel. Neither orthopyroxene nor clinopyroxene are present in these rocks, possibly reflecting bulk composition of the protolith. P-type (Cr-bearing) majorite occurs in a rare garnet peridotite xenolith as crystals up to 30 μm in diameter that form part of a symplectite reaction microstructure with grains of Al-Mg spinel (Fig. 3, B and C). The spinel is similar in composition to high-

Table 2. Compositions of prograde reactants in sample KC-99-M3.

Mineral:	Majorite			UHP majorite?			Spinel		Garnet	
Spot no. or reference:	#59	#57	#56	#44	#161	#159	#51	#160	#53	#54
SiO_2	46.72	46.42	51.72	48.04	41.03	40.56	0.23	0.29	41.18	41.74
TiO_2	0.69	0.71	0.72	0.45	3.20	4.09	0.37	0.27	0.56	0.56
Al_2O_3	12.49	14.91	5.37	10.05	16.00	15.60	59.87	58.20	23.18	23.05
Cr_2O_3	0.05	0.07	0.00	0.02	0.01	0.05	0.13	0.17	0.05	0.03
FeO	12.98	12.92	12.86	13.93	10.01	10.87	24.60	25.77	11.55	11.81
MnO	0.45	0.33	0.41	0.36	0.16	0.16	0.24	0.32	0.36	0.23
MgO	23.89	23.95	26.80	24.22	14.54	14.27	16.13	15.77	18.44	18.16
CaO	2.32	1.39	1.80	1.81	9.75	9.45	0.01	0.00	4.33	3.72
NiO	0.08	0.02	0.00	0.00	0.08	0.00	0.01	0.07	0.00	0.00
Na_2O	0.00	0.07	0.02	0.12	3.04	3.29	0.00	0.00	0.04	0.06
K_2O	0.01	0.00	0.00	0.00	1.64	1.14	0.00	0.00	0.00	0.00
Total	99.67	100.79	99.70	99.01	99.47	99.46	101.60	100.87	99.69	99.36
Cations per:	12 oxygen						4 oxygen		12 oxygen	
Si^{4+}	3.378	3.302	3.716	3.501	3.081	3.053	0.006	0.006	2.970	3.012
Ti^{4+}	0.037	0.038	0.039	0.025	0.181	0.232	0.007	0.005	0.030	0.030
Al^{3+}	1.064	1.250	0.455	0.864	1.416	1.384	1.825	1.796	1.970	1.960
Cr^{3+}	0.003	0.004	0.000	0.001	0.001	0.003	0.003	0.004	0.003	0.001
Fe^{2+}	0.785	0.769	0.773	0.849	0.628	0.684	0.532	0.564	0.697	0.713
Mn^{2+}	0.028	0.020	0.025	0.022	0.010	0.010	0.005	0.007	0.022	0.014
Mg^{2+}	2.575	2.539	2.871	2.631	1.628	1.601	0.622	0.615	1.983	1.953
Ca^{2+}	0.180	0.106	0.138	0.142	0.784	0.762	0.000	0.000	0.334	0.287
Na^{+}	0.000	0.009	0.002	0.017	0.443	0.480	0.000	0.000	0.006	0.009
K^{+}	0.001	0.000	0.000	0.000	0.157	0.109	0.000	0.000	0.000	0.000
Total	8.051	8.037	8.019	8.051	8.330	8.317	3.000	2.999	8.016	7.981

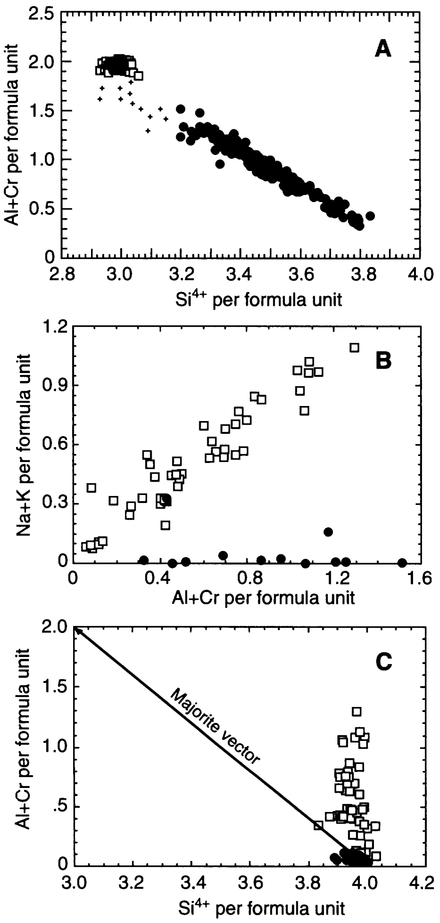

Fig. 2. (**A**) Chemical structural data based on 12 oxygens pfu for garnets from Malaita. Garnets exhibit an extreme range of pressure induced covariation between Si and Al+Cr and define a well correlated trend between pyrope (open squares) with Si = 3 pfu and Al+Cr = 2 pfu and ideal clinopyroxene (*19*) with Si^{4+} = 4 pfu and Al+Cr = 0 pfu. Slope of the combined vector defines continuous solid solution in majoritic compositions (solid circles) from 3.2 Si pfu to 3.8 Si pfu, reflecting the presence of Si^{4+} in octahedral coordination. A small population of ~3 Si pfu "garnets" (crosses) are clearly deficient in Al+Cr (1.85 to 1.55). These may be the ultradeep "majorite" composition reported in experiments at 27 GPa (*23*, *24*), which forms at depths of ~670 km. (**B**) Data relative to 12 oxygen atoms for aluminous pyroxene diamond inclusions (open squares) from kimberlites (*5*, *6*, *28*, *53*, *59*) and representative majorite compositions (solid circles) from Tables 1 and 2. The clinopyroxene data show the expected jadeite substitution vector yielding a slope similar to unity. By contrast, Al and Cr in the majoritic garnets are not balanced by Na and K substitutions. Majorite substitution into garnet mainly involves the M^{2+} cations (Fe, Ca, and Mg). (**C**) Si versus Al+Cr variation in diamond inclusion clinopyroxenes (open squares) and orthopyroxenes (solid circles) (*5*, *6*, *28*, *53*, *59*). The clinopyroxenes have an average Si^{4+} pfu of 3.94 ± 0.08 and do not plot on the majorite vector. Rather they define a much steeper vector because Al incorporation has evidently no effect on the Si content of pyroxene. Orthopyroxenes from diamond inclusions or kimberlite-hosted xenoliths are invariably much more siliceous than Malaita majoritic garnets. They have low contents of Al and Cr, and there is no evidence for solid solution toward a more aluminous orthopyroxene.

Table 3. Compositions of ultrahigh pressure minerals from Malaita compared to literature data.

Mineral:	Mg-perovskite?		Ca-perovskite?				UHP majorite		Spinel			Aluminous phase			
Occurrence:	Malaita	São Luiz	Malaita				Malaita	Exper.	Malaita		Monastery	Malaita		Experiment	
Sample number:	KC-98-16	BZ210B	KC-98-8	KC-98-17A	KC-98-16#23	KC-98-15#29	KC-98-16	Mj 27 GPa	KC-98-B	KC-98-B	M1A	KC-98-18	KC-98-17A	Al phase 27 GPa	Al phase 27 GPa
Reference:	This work	(*7*)	This work	This work	This work	This work	This work	(*23*)	This work	This work	(*28*)	This work	This work	(*34*)	(*23*)
SiO_2	53.26	51.41	44.37	48.04	51.50	52.61	43.01	41.51	0.09	0.06	0.00	25.11	23.39	23.42	26.96
TiO_2	0.05	0.02	2.48	2.58	0.29	0.30	0.91	2.02	0.11	0.19	0.19	0.33	0.26	0.38	0.92
Al_2O_3	4.57	10.04	12.44	6.07	4.09	4.15	13.18	19.79	60.56	65.22	59.63	37.47	40.14	46.67	32.78
Cr_2O_3	0.45	1.19	0.05	0.07	1.05	1.09	1.58	0.15	0.76	0.63	0.07	0.03	0.17	–	0.10
Fe_2O_3	–	–	–	–	–	–	–	–	6.66	2.34	6.10	–	–	–	–
FeO	7.67	5.28	7.54	7.14	2.61	2.59	4.73	16.50	14.69	12.57	21.66	14.95	13.95	3.10	16.19
MnO	0.42	0.93	0.18	0.28	0.08	0.07	0.06	0.08	0.30	0.18	0.52	0.27	0.22	–	0.05
MgO	30.10	30.21	11.48	14.75	15.77	15.53	18.18	11.44	17.63	19.57	12.91	21.67	21.66	18.53	10.74
CaO	1.58	0.65	19.05	20.63	20.13	20.32	10.16	3.75	0.00	0.00	–	0.88	0.60	3.10	1.87
NiO	0.02	0.02	0.00	0.00	0.01	0.07	0.11	0.00	0.01	0.04	–	–	–	–	–
Na_2O	0.20	1.05	1.99	0.26	2.33	2.28	4.53	5.07	0.00	0.02	–	0.03	0.04	4.71	11.15
K_2O	0.07	0.26	0.17	0.02	0.00	0.00	0.63	0.05	0.00	0.00	–	0.01	0.02	–	–
Total	98.39	101.06	99.75	99.85	97.85	99.04	97.08	100.36	100.81	100.81	101.08	100.76	100.45	99.91	100.73
Cations per:	3 oxygen						12 oxygen		4 oxygen			12 oxygen			
Si^{4+}	0.947	0.886	0.829	0.893	0.957	0.964	3.237	3.092	0.002	0.002	0.000	1.849	1.720	1.673	2.077
Ti^{4+}	0.001	0.000	0.035	0.036	0.004	0.004	0.052	0.113	0.002	0.004	0.004	0.018	0.014	0.020	0.053
Al^{3+}	0.096	0.204	0.274	0.133	0.090	0.090	1.169	1.737	1.846	1.934	1.868	3.251	3.479	3.928	2.976
Cr^{3+}	0.006	0.016	0.001	0.001	0.015	0.016	0.094	0.009	0.016	0.012	0.001	0.002	0.010	–	0.006
Fe^{3+}	–	–	–	–	–	–	–	–	0.130	0.044	0.122	–	–	–	–
Fe^{2+}	0.114	0.076	0.118	0.111	0.041	0.040	0.298	1.028	0.318	0.265	0.482	0.920	0.858	0.185	1.043
Mn^{2+}	0.006	0.014	0.003	0.004	0.001	0.001	0.004	0.005	0.007	0.004	0.012	0.017	0.014	–	0.003
Mg^{2+}	0.797	0.776	0.320	0.409	0.437	0.424	2.039	1.270	0.680	0.734	0.512	2.378	2.374	1.973	1.233
Ca^{2+}	0.030	0.012	0.381	0.411	0.401	0.399	0.820	0.299	–	–	–	0.069	0.047	0.237	0.154
Ni^{2+}	0.001	0.001	0.000	0.000	0.000	0.002	0.013	0.000	–	0.001	–	–	–	–	–
Na^{+}	0.007	0.035	0.072	0.009	0.084	0.081	0.661	0.732	–	0.001	–	0.004	0.006	0.652	1.665
K^{+}	0.002	0.006	0.004	0.001	0.000	0.000	0.061	0.005	–	–	–	0.001	0.002	–	–
Total	2.006	2.025	2.037	2.009	2.029	2.021	8.448	8.290	3.000	3.000	3.000	8.509	8.525	8.669	9.211
Mg/(Mg+Fe)	0.875	0.911	0.731	0.786	0.915	0.914	0.873	0.553	0.681	0.735	0.515	0.721	0.735	0.914	0.542

pressure spinel reported by Liu (*22*). This microstructure is interpreted to have developed from breakdown of an even higher pressure prograde assemblage of Ca-perovskite, Mg-perovskite, and a phase low in Si and high in Ti and Na that is similar to the ultrahigh pressure "majorite" composition reported in experiments at 27 GPa (Fig. 3B) (*23, 24*). Development of the majorite-spinel symplectite microstructure may reflect slow decompression during long time-scale convection in the mantle transition zone. This process and evidence for metastable survival may explain the range of majorite compositions within single xenoliths (*18*). Relationships shown in Fig. 3, B and C demonstrate that formation of the symplectite predated development of glassy kelyphite veins which formed by decompression melting during rapid ascent of the host alnöite. At high scanning electron microscope (SEM) magnification, all high-pressure phases, including those with majoritic chemistry, appear as a very fine grained (submicrometer) polycrystalline aggregate (Fig. 3, D and E). This groundmass also appears to contain relics of resorbed reactant phases. Formation of the fine-grained polycrystalline groundmass is interpreted to be caused by rapid decompression during eruption that induced partial reversion and subsequent reordering.

Majorite is a complex garnet solid solution between pyrope-almandine and orthopyroxene or clinopyroxene that forms at pressures between $\sim$12 and 26 GPa in both basaltic and peridotitic protoliths. With increasing pressure, garnet with $\sim$3 Si^{4+} atoms pfu becomes progressively depleted in Al and enriched in Si (up to 3.83 Si^{4+} pfu), M^{2+} (Ca^{2+} + Mg^{2+} + Fe^{2+}) cations, and Na^{+} (*25–27*). Majorite has occasionally been observed as rare inclusions in diamond (*28*). Intergrowths of garnet and clinopyroxene or orthopyroxene in eclogite and peridotite xenoliths have been reported from a number of cratonic kimberlite pipes (*3, 4*) and from units of garnet-pyroxenite and garnet peridotite in obducted ultramafic units in orogenic belts. These intergrowths have been interpreted to be pyroxene exsolved from majoritic garnet (*29*). The occurrence of majorite is significant, because this phase is considered to be a dominant constituent of the transition zone between depths of 400 and 650 km (*25, 26, 30–35*).

Compared to all other reported natural majorites, the Malaita majorites include significantly more silicic (Si^{4+} up to 3.83 pfu) compositions and are thus interpreted to have been derived from much greater depths. These majorites appear to have low first-order (gray) birefringence, possibly indicating that their structure deviates from cubic symmetry (*36*). Malaita xenoliths provide the first opportunity to directly study the composition and mineralogy of the mantle transition zone and its lower mantle boundary in the pressure range of $\sim$12 to 27 GPa.

Other High-Pressure Phases

Experiments imply that in the pressure range between 15 and 22 GPa, E-type majorite is accompanied by metastable pyrope and stishovite (*25*). At even greater depths between 22 and 27 GPa, both E- and P-type majorite react to form a less silicic phase with 3.18 to 3.32 Si atoms for 12 oxygens that was still termed majorite by (*23*) [but see (*24*)]. A small population of "garnets" (Fig. 2A) with $\sim$3 Si pfu, but clearly deficient in Al+Cr (1.85 to 1.55), may be this ultradeep aluminous phase that forms at depths of $\sim$670 km. In experiments at pressures >22 GPa, these "ultrahigh pressure majorites" coexist with Ca silicate perovskite. At pressures >24 GPa, several enigmatic aluminous phases appear, and at pressures >25.5 GPa, Mg-Al silicate perovskite becomes a stable phase (*22, 23, 26, 31, 32, 34, 37, 38*). All of these phases occur in the Malaita samples (Table 3) and are comparable in composition to those synthesized by (*23*) between 24 and 27 GPa.

Other high-pressure phases in Malaita samples include pyroxene-ilmenite-rutile intergrowths (*39*), jadeite-rich clinopyroxene, picroilmenite (MgO, 3.55% to 8.31%), large ($\sim$2 cm by 1 cm) "kimberlitic" zircons, Fe-Ni sulfides, a SiO$_2$ phase, and microdiamond surrounded by narrow rims of graphite. A SEM image of one of the microdiamonds that occurs as an inclusion in E-type pyrope and compositional profiles for Si, Mg, Ca, and Fe are shown in Fig. 4. The presence of Fe and Ca in the analytical profile of the diamond is interpreted to arise from the transmission of x-rays through the diamond into the garnet substrate. The pref-

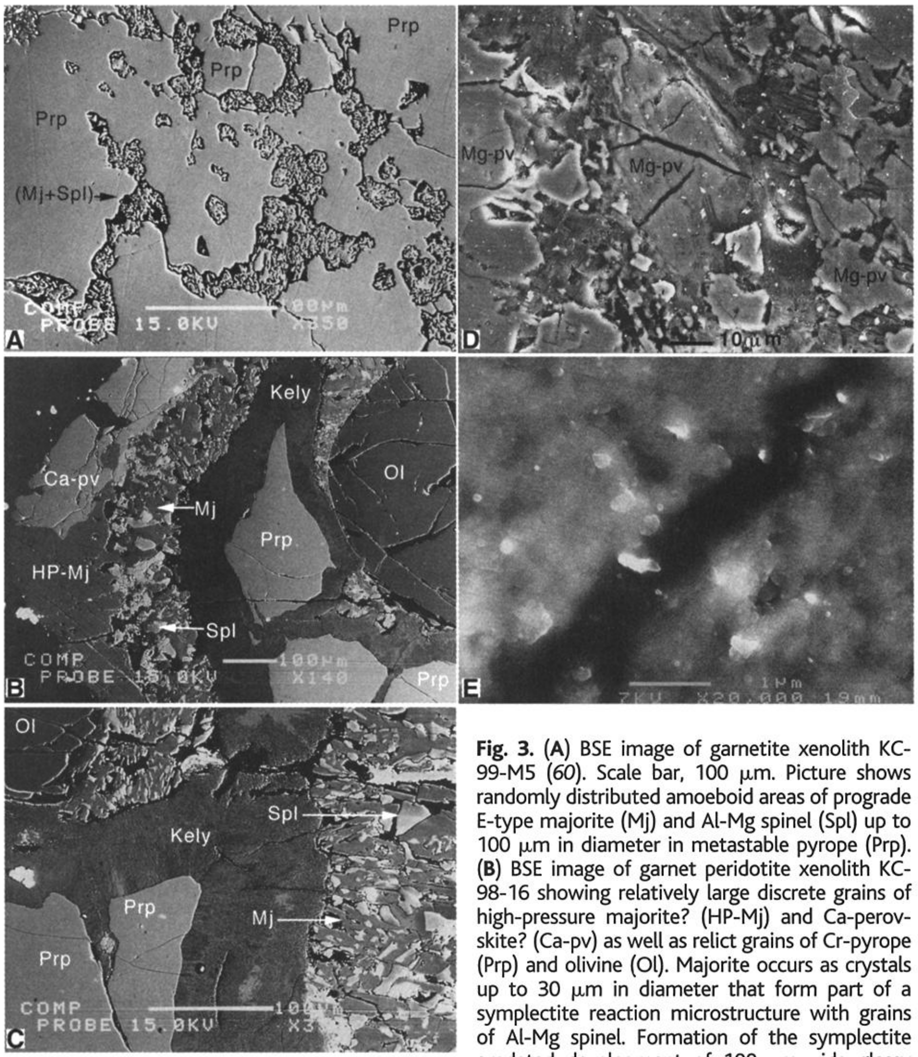

Fig. 3. (**A**) BSE image of garnetite xenolith KC-99-M5 (*60*). Scale bar, 100 μm. Picture shows randomly distributed amoeboid areas of prograde E-type majorite (Mj) and Al-Mg spinel (Spl) up to 100 μm in diameter in metastable pyrope (Prp). (**B**) BSE image of garnet peridotite xenolith KC-98-16 showing relatively large discrete grains of high-pressure majorite? (HP-Mj) and Ca-perovskite? (Ca-pv) as well as relict grains of Cr-pyrope (Prp) and olivine (Ol). Majorite occurs as crystals up to 30 μm in diameter that form part of a symplectite reaction microstructure with grains of Al-Mg spinel. Formation of the symplectite predated development of 100-μm-wide glassy kelyphite veins, which formed by decompression melting during rapid ascent of the host alnöite. Scale bar, 100 μm. (**C**) BSE image of garnet peridotite xenolith KC-98-16 at higher magnification showing details of the Mj-Spl symplectite microstructure and discordant relationships with the decompression induced kelyphytic glass that contains remnants of reactant phases. Scale bar, 100 μm. (**D**) SE image of phases with Mg-perovskite chemistry in garnet peridotite xenolith KC-98-16. Scale bar, 10 μm. (**E**) SE image of phases with Mg-perovskite chemistry at high magnification showing relics of resorbed reactant phases in a submicrometer polycrystalline groundmass that is interpreted to be caused by rapid decompression during eruption that induced partial reversion and reordering. Scale bar, 1 μm.

erence for Fe and Ca rather than Si and Mg is related to the x-ray transmission characteristics of diamond, which transmits shorter wavelength x-rays more efficiently than those with longer wavelengths (*40*).

Infrared Spectroscopy of Ultrahigh Pressure Materials

The infrared reflectance spectrum of the phase with Mg perovskite-chemistry in the garnet peridotite xenolith (Table 3) is shown in Fig. 5A, where it is compared with spectra of diopside and enstatite (*41*). The perovskite-chemistry phase has broad reflectance peaks near 960 and 880 cm^{-1}, which are associated with stretching vibrations of silica tetrahedra, and weaker bands between 600 and 700 cm^{-1}, which are probably associated with Si-O-Si bending vibrations (*42, 43*). The peaks in the spectrum of the phase with Mg-perovskite chemistry are substantially broadened relative to the peaks that lie at grossly similar frequencies in the pyroxene samples. Moreover, there are mutually exclusive features between the spectra, such as the absence of a discrete peak at 990 to 1010 cm^{-1} in the analyzed sample and the presence of the feature near 740 cm^{-1}. Indeed, the reflectance spectrum of the perovskite chemistry phase is substantially different from those of the pyroxenes. This difference cannot be attributed to particle-size effects, because the change in the reflectance spectra of pyroxenes due to particle size reduction is different from those documented in Fig. 5A (*44*). At higher frequencies (>~1100 cm^{-1}), there is clear evidence for a scattering background in the spectrum, implying that local heterogeneities are present at scale lengths of several micrometers and smaller (Fig. 3E). Given the breadth of the features in the spectrum, the most plausible interpretation is that the phase with Mg-perovskite chemistry represents a disordered material with pyroxene stoichiometry. This is consistent with the likely presence of silicate chains within the material, based on the gross similarity of the positions of the reflectance peaks above 800 cm^{-1} with those of pyroxenes. The presence of such a disordered, silicate chain-containing material in these samples is not surprising: the single other observation of naturally occurring reverted silicate perovskite shows the clear presence of a disordered phase of pyroxene stoichiometry (*45*). We believe that the present observations are analogous to the meteoritic results (albeit with reversion having likely occurred on a substantially longer time scale in the xenolith samples).

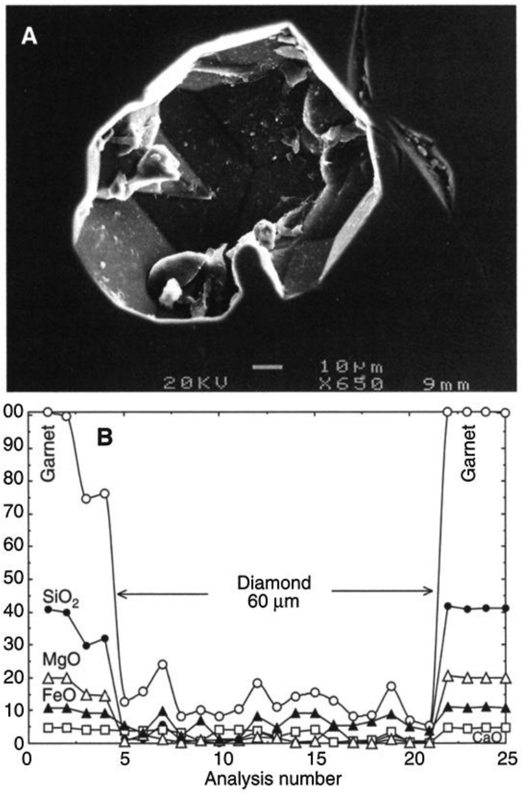

Fig. 4. (**A**) An SE image of a microdiamond from KC-98-M35 that occurs as an inclusion in E-type pyrope. Scale bar, 10 µm. (**B**) Electron microprobe compositional profiles for Si, Mg, Ca, and Fe across microdiamond. The Fe and Ca counts are likely produced in the garnet substrate and are observed relative to the lighter elements, because of preferential transmission through diamond of shorter wavelength x-rays (*40*). In addition to the probe results, Raman spectroscopy has also confirmed that this phase is carbon.

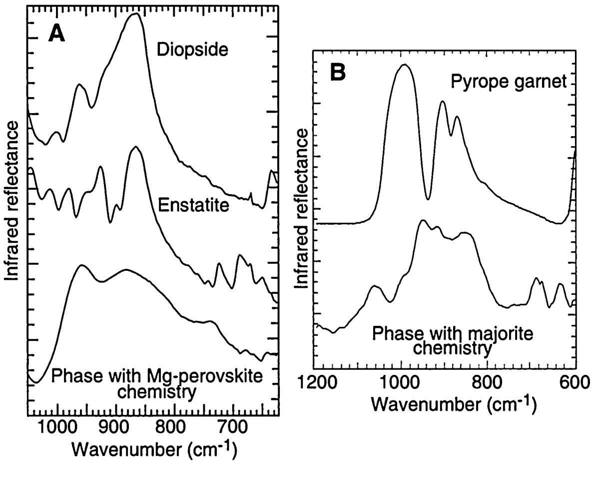

Fig. 5. (**A**) Unpolarized infrared reflectance spectra of thin sections of natural samples of diopside (from Bird Creek, Ontario), enstatite (Bamble, Norway) and of a 50-µm-diameter spot in the vein of perovskite chemistry within sample KC-98-16. Although the relative amplitudes of peaks may vary depending on crystallographic orientation of the sample material, both the magnitude of broadening and the comparatively small number of reflectance peaks in the spectrum of the vein of perovskite chemistry indicate that substantial disorder is present within this sample. (**B**) Unpolarized infrared reflectance spectrum of a 50-µm-diameter spot of pyropic garnet from sample KC-98-M35 compared with a comparable spot size in the majorite-chemistry region of sample KC-98-16. The spectrum of pyropic garnet is in accord with previous spectra of garnets near the pyrope-almandine join (*61*). In contrast, the spectrum of the majorite-chemistry region shows some similarity to those of chain silicates (*43*), indicating that some high temperature reversion of this material has taken place.

It is well known that at ambient pressures and laboratory time scales, magnesium silicate perovskite reverts to an amorphous phase or enstatite at temperatures of 750 to 850 K (*46*). Similarly, small particles of glasses of pyroxene composition have been observed to form from perovskite in ~300 hours at 1073 K, and in 7 min at 1273 K (*47*). Over shorter time scales, broadened pyroxene-like peaks are observed in disordered samples quenched from high-temperature conditions (*47*). These results are in general accord with those shown in Fig. 5A and provide a likely genetic history for the formation of high-pressure phases in the xenoliths. We interpret this to involve initial reversion (during ascent) of perovskite to an amorphous phase, followed by subsequent (and partial) temperature-induced ordering of the amorphous material. The degree of ordering/microstructural development within these samples may ultimately provide a constraint on their time-temperature-transformation history during ascent from depth.

The spectra of the zones of majorite chemistry have some similarities with that of MgSiO$_3$-clinoenstatite (*43*), although as with the zones of perovskite-chemistry, the peaks are significantly broadened and moderately shifted relative to the end-member. Specifically, $MgSiO_3$-clinoenstatite has peaks at 1074, 1017, 951, 900, 860, and 690 cm^{-1}. In the spectrum shown in Fig. 5B, the comparatively sharp features at 1017 and 900 cm^{-1} are absent (or broadened into weak shoulders), and the peaks at 1055, 960, and 858 cm^{-1} are significantly broadened relative to the end-member spectrum (this broadening is not a consequence of comparing the reflectance spectra of Fig. 5B with the absorbance spectra of (*43*), as Kramers-Kronig transforms of the spectra of Fig. 5B retain substantially broadened peaks). In this instance, the broadening could be produced by a combination of Al substitution in the clinopyroxene and significant structural disorder within the material induced by reversion from a high-pressure garnet phase. Unfortunately, few data exist on the effect of Al on the infrared spectra of clinopyroxenes, and the resultant degree of "transformational" disorder is difficult to assess.

Majorite Geobarometer

Substitution of Si for Al+Cr with increasing pressure can be used as a geobarometer of equilibration in the mantle (Fig. 6A) (*4, 30*). Exchange between Si and Al+Cr for the experimental data is well correlated with the range of substitutions shown by the Malaita majorites (Fig. 6B). The highest pressure experimental compositions show the highest Si pfu and lowest Al+Cr pfu. We have developed empirical geobarometers for both substitutions from published data (*48*). Very good agreement between Si and Al+Cr substitution in the natural and synthetic datasets demonstrates that these barometers are applicable to both P- and E-type majorites. The barometers are P (GPa) $= -50.7 + 18.97(\mathrm{Si})$ [$r^2 = 0.886$] (Fig. 6C) and P (GPa) $= 23.7 - 9.06(\mathrm{Al+Cr})$ [$r^2 = 0.890$] (Fig. 6D).

Pressures calculated from the experimental data using each barometer agree to better than 1 GPa [$r^2 = 0.987$] (Fig. 6E). The barometers are apparently independent of temperature, and calculated pressures are in good agreement with those determined in experiments (Fig. 6F). For the total Malaita population (Fig. 6G), average agreement between P(Si) and P(Al+Cr) is ±0.5 GPa. The uncertainty is within analytical error and reflects largely the quality of mineral chemical data. The barometer implies that the majorite-bearing Malaita xenoliths and macrocrysts are derived from the deep upper mantle in the pressure-depth interval 9.5 GPa (260 km) to 22 GPa (570 km).

Discussion

A paleogeotherm at ~34 Ma for the Ontong Java Plateau has previously been determined from pyroxene geothermobarometry for samples from Malaita (*14, 17*). The paleogeotherm is considerably hotter than typical cratonic geotherms and indicates that diamond could not have been stable in the Ontong Java Plateau lithospheric mantle, or oceanic lithosphere in general, during either the eruption of the Ontong Java Plateau basalts or that of the ~34 Ma alnöites. Diamond could, however, have been stable at depths >150 km. In fact, microdia-

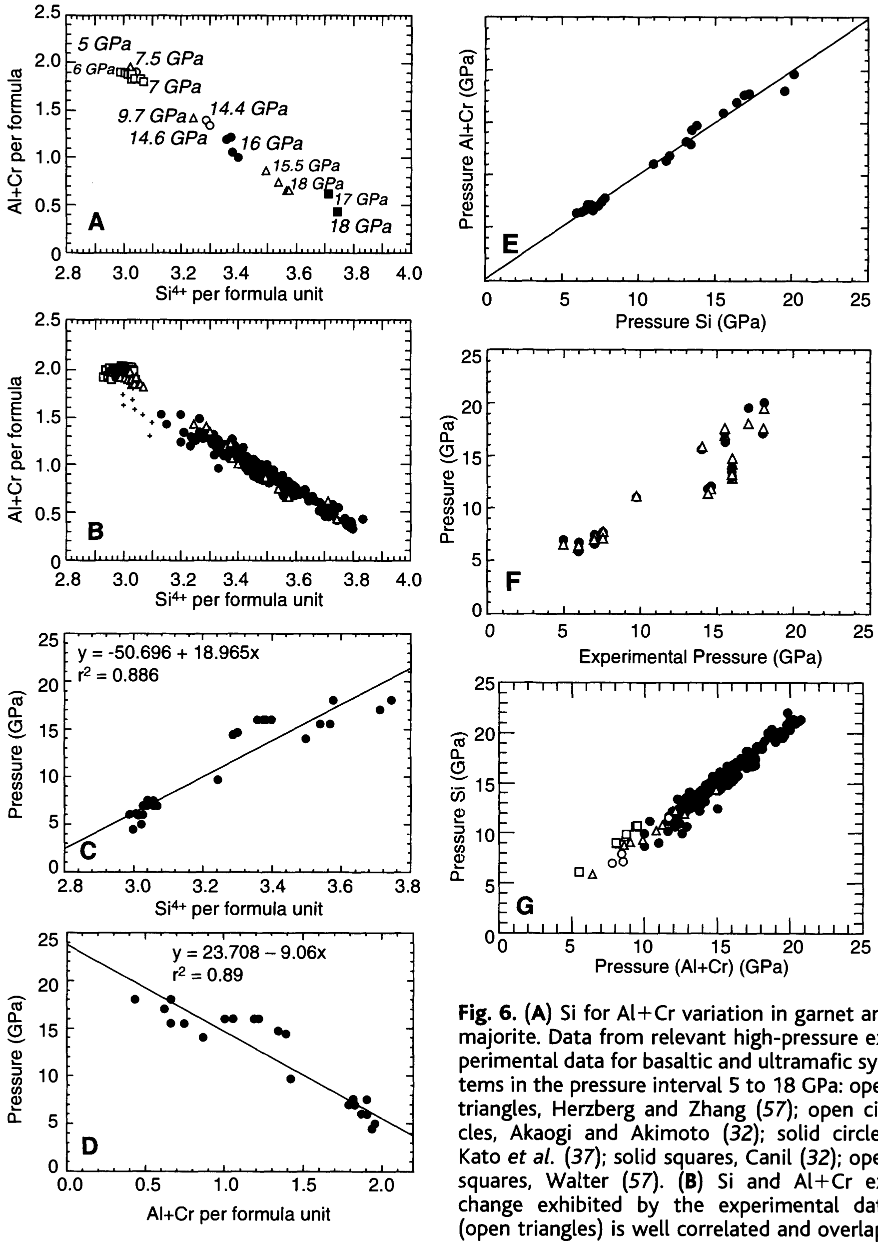

Fig. 6. (**A**) Si for Al+Cr variation in garnet and majorite. Data from relevant high-pressure experimental data for basaltic and ultramafic systems in the pressure interval 5 to 18 GPa: open triangles, Herzberg and Zhang (*57*); open circles, Akaogi and Akimoto (*32*); solid circles, Kato *et al.* (*37*); solid squares, Canil (*32*); open squares, Walter (*57*). (**B**) Si and Al+Cr exchange exhibited by the experimental data (open triangles) is well correlated and overlaps the range of substitutions shown by the Malaita majorites, with the highest pressure experimental compositions showing highest Si pfu and lowest Al+Cr pfu. (**C**) Correlation between experimentally determined Si^{4+} pfu and quoted experimental pressure estimates. Linear regression of the data yields the following empirical barometer: P (GPa) $= -50.7 + 18.97(\mathrm{Si})$. (**D**) Correlation between experimentally determined Al+Cr pfu and quoted experimental pressure estimates. Linear regression of the data yields the following empirical barometer: P (GPa) $= 23.7 - 9.06(\mathrm{Al+Cr})$. (**E**) Comparison of pressures calculated using the empirical Si and (Al+Cr) barometers. Methods agree to better than 1 GPa [$r^2 = 0.987$]. (**F**) Comparison of experimental pressure estimates, and pressures calculated using the Si barometer (solid circle) and (Al+Cr) barometer (open triangle). (**G**) Pressure estimates for Malaita majorite-bearing xenoliths and macrocrysts. Shown for comparison are pressures calculated for majorite diamond inclusions reported from Monastery Mine (*28*) (open triangles) and Jagersfontein (*53*) (open circles) and majorite reconstituted from garnet-clinopyroxene (orthopyroxene) intergrowths in xenoliths from Jagersfontein (*3, 4*) (open squares). Pressures calculated for majorite diamond inclusions lie along the same vector as the Malaita majorites and yield a maximum of 15 GPa. Note that the majorite compositions from reconstituted xenoliths yield systematically higher pressures by the Si barometer than the (Al+Cr) barometer. This suggests that SiO_2 or (Al_2O_3+Cr_2O_3) in the garnet and pyroxene mixing proportions for the xenoliths (*3, 4*) were overestimated.

monds do occur in pyrope and majorite-bearing Malaita garnet macrocrysts and majorite-bearing E-type garnetite xenoliths. This observation confirms that diamonds are present at least locally in the transition zone (*49*). E-type diamond in this tectonic setting could only have formed during subduction of the eclogitic precursor or during (transient) storage of slabs in the transition zone (*33, 50*).

Previous studies have interpreted Malaita alnöites to have formed by fractional crystallization of a proto-alnöitic magma in the asthenosphere (*16, 17, 51*). Malaita peridotite xenoliths, rare eclogite xenoliths, and a diverse suite of ilmenite, garnet, pyroxene, and zircon macrocrysts were interpreted to indicate maximum source depths of ~140 km (*10, 12, 14, 16, 17, 51, 52*). However, the occurrence of majoritic and microdiamond-bearing xenoliths and macrocrysts forming from Mg-Si perovskite-bearing precursors, clearly requires the source of the host alnöite to be deeper than 670 km in the lower mantle (*50*) or some major upward transport of material before eruption. Thus, macrocrysts do not form by an unconstrained fractional crystallization process of the alnöitic magma at the interface between the lithospheric and asthenospheric mantle (*16*).

Malaita's Si-rich majorite-bearing xenoliths and macrocrysts are derived from depths of up to 570 km (22 GPa), which is significantly deeper than majorite diamond inclusions reported from Monastery Mine (*28*) and Jagersfontein (*53*), namely, 9 GPa (262 km) to 15 GPa (413 km) and 7 GPa (204 km) to 11 GPa (303 km) determined using the barometer we present here (Fig. 6G). Additional high-pressure phases from Malaita such as Ca and Mg-Si perovskite indicate substantially greater depths (770 km).

The presence of TiO_2- and Na_2O-rich eclogitic pyropes in the Malaita garnetite xenoliths, with compositions identical to E-type garnets in diamond inclusions, indicates significant metastable preservation of pyrope garnet in the transition zone. Such preservation could occur because temperatures in subduction zones are relatively low. In addition, the ultradeep slabs may be anhydrous, and the resultant amount of chemical interaction between pyrope and pyroxene could be limited by lithology and/or kinetics. The existence of such metastability in the transition zone suggests that inferences based on silicate minerals that occur as diamond inclusions may underestimate the depth of formation of diamond. In other words, the apparent absence of majorite does not preclude formation of diamond in the mantle transition zone.

Metastability may also be significant for the interpretation of the seismic structure of the mantle. The region above the base of the upper mantle is defined seismically by extremely rapid seismic velocity increases (*54*) and by compressional and shear-wave velocities that progressively increase from ~9.5 to 10 km/s for *P* waves and 5.0 to 5.5 km/s and *S* waves, respectively (*55*). The progressive change in seismic velocities could reflect the fact that kinetically inhibited phase transformations are unlikely to occur at specific depths. Also, the preponderance of E-type ultradeep xenoliths indicates that the mantle transition zone which was first cut by the Ontong Java Plateau plume and subsequently sampled by lower mantle-derived alnöites is likely to be dominated by subducted oceanic crust. This appears to be confirmed by seismic tomographic images for the southwestern Pacific region that clearly show a zone of high seismic velocities lying east of New Guinea (*56*). This may represent the site of accumulation of subducted Pacific oceanic crust. The other significant interpretation from the southwestern Pacific/south Asian mantle tomography (*56*) is that at 400 km depth, the transition zone is not uniformly cool. Instead, it exhibits very pronounced lateral gradients in temperature and possibly also in mineralogy. The transition zone may therefore represent a thermally and compositionally variable, yet volumetrically extremely significant geochemical mantle reservoir.

References and Notes

1. S. E. Haggerty, *J. Geodyn.* **20**, 331 (1995).
2. P. H. Nixon, Ed., *Mantle Xenoliths* (Wiley, New York, 1987).
3. S. E. Haggerty and V. Sautter, *Science* **248**, 993 (1990).
4. V. Sautter, S. E. Haggerty, S. Field, *Science* **252**, 827 (1991).
5. H. O. A. Meyer and H.-M. Tsai, *Miner. Sci. Eng.* **8**, 242 (1976).
6. H. O. A. Meyer and D. P. Svisero, in *Physics and Chemistry of the Earth*, L. H. Ahrens, J. B. Dawson, A. R. Duncan, A. J. Erlank, Eds. (Pergamon, New York, 1975), vol. 9, pp. 785–795; J. J. Gurney, J. W. Harris, R. S. Rickard, R. O. Moore, *Trans. Geol. Soc. S. Afr.* **88**, 301 (1985).
7. C. McCammon, M. Hutchison, J. Harris, *Science* **278**, 434 (1997); L. G. Liu, *Contrib. Mineral. Petrol.* **134**, 170 (1999); R. M. Davies *et al.*, *Diamonds from the Deep: Pipe DO-27, Slave Craton, Canada*, Proceedings of the 7th International Kimberlite Conference, J. B. Dawson volume (vol. 1), 13 to 17 April, 1998, Cape Town, South Africa, J. J. Gurney, J. L. Gurney, M. D. Pascoe, S. H. Richardson, Eds. (Red. Roof Design, Cape Town, South Africa), pp. 148–155.
8. S. E. Haggerty, *Science* **285**, 851 (1999).
9. Alnöite is the name given to silica-undersaturated, highly alkaline rocks that were first described from the island of Alnö, Sweden. However, in terms of chemistry, mineralogy, and texture, alnöites are very similar to kimberlites. Kimberlites are potassic ultrabasic hybrid rocks containing megacrysts. They typically occur as pipes, sills, or dykes. Because kimberlites were believed to be restricted to continental areas, kimberlite-like rocks from oceanic environments were called alnöites. We suggest that the latter term be abandoned in favor of kimberlite.
10. C. R. Neal, J. J. Mahoney, L. W. Kroenke, R. A. Duncan, M. G. Petterson, Eds., *The Ontong Java Plateau* (*Geophys. Monogr. 100*, American Geophysical Union, Washington, DC, 1997), pp. 183–216.
11. L. W. Kroenke, *Hawaii Inst. Geophys. Rep. HIG-72-5* (1972), p. 119.
12. P. H. Nixon, *Nature* **287**, 718 (1980).
13. P. J. Coleman and L. W. Kroenke, *Geo-Marine Lett.* **1**, 129 (1981); M. G. Petterson *et al.*, *Tectonophysics* **283**, 1 (1997).
14. P. H. Nixon and F. R. Boyd, in *The Mantle Sample: Inclusions in Kimberlites and Other Volcanic Rocks*, Proceedings of the 2nd International Kimberlite Conference, October 1977, Santa Fe, NM, F. R. Boyd and H. O. A. Meyer, Eds. (American Geophysical Union, Washington, DC, 1979), vol. 2, pp. 400–423.
15. Samples were provided by Zorba Mining & Exploration Support Pty. Ltd. and by A. Sasako, Minister for State Assisting the Prime Minister of the Solomon Islands.
16. C. R. Neal and J. P. Davidson, *Geochim. Cosmochim. Acta* **53**, 1975 (1989).
17. P. H. Nixon and C. R. Neal, in (*2*), pp. 335–345.
18. The majority of analyses were carried out in the Centre for Microscopy and Microanalysis (CMM) at the University of Queensland, using a JEOL Super Probe equipped with wavelength-dispersive spectrometers. The microprobe was operated with an accelerating voltage of 15 kV, a current of 15 nA, and a spot size of 10 to 20 μm. Duplicate analyses of a small number of samples were also undertaken using an energy-dispersive detector on a JEOL SEM at the Queensland University of Technology. Both instruments were calibrated with mineral and oxide standards. No differences were observed in quality of analyses using different techniques. The mean and standard deviation of analyses (n = 9) of Kakanui pyrope mineral standard obtained during this study are presented in Table 1. Kakanui pyrope analyses exhibit excellent stoichiometry, namely, 2.969 ± 0.008 Si^{4+} and 8.008 ± 0.008 total cations pfu. The high precision achieved in this study (as exhibited by Si^{4+} and Al+Cr, namely, 1.996 ± 0.015 pfu) is required to assess the quality of majorite analyses. Web table 1 is available at www.sciencemag.org/feature/data/1049485.shl.
19. Clinopyroxenes from high-pressure xenoliths invariably contain Al and Cr (unlike the "ideal" composition that is used to define the majorite vector). A mixture between coexisting pyrope and clinopyroxene in real xenoliths would therefore not plot on the majorite vector defined in Fig. 2A. See also Fig. 2B.
20. D. Perkins, T. J. B. Holland, R. C. Newton, *Contrib. Mineral. Petrol.* **78**, 99 (1981); T. Gasparik and R. C. Newton, *Contrib. Mineral. Petrol.* **85**, 186 (1984).
21. G. P. Brey, T. Köhler, K. G. Nickel, *J. Petrol.* **31**, 1313 (1990).
22. L.-G. Liu, *Earth Planet. Sci. Lett.* **41**, 398 (1978).
23. K. Hirose, Y. W. Fei, Y. Z. Ma, H. K. Mao, *Nature* **397**, 53 (1999).
24. When recalculated to 12 oxygen pfu, stochiometry is poor; i.e., total cations are 8.4 to 8.45 both for our analyses and those of (*23*). However, when recalculated on the basis of 10 oxygen pfu, total cations = ~7 pfu. This may suggest that at pressures of 27 GPa (*23*), majorite sensu stricto is no longer stable and is replaced by a new mineral. To remain consistent with nomenclature of (*23*), we refer to this aluminous phase as ultrahigh pressure "majorite."
25. A. E. Ringwood, in *Kimberlites and Related Rocks: Their Composition, Origin and Emplacement*, J. Ross *et al.*, Eds. (Geological Society of Australia Special Publication No. 14, Perth, Australia, 1989), vol. 1, pp. 457–485.
26. T. Irifune, W. O. Hibberson, A. E. Ringwood, in *Kimberlites and Related Rocks: Their Mantle/Crust Setting, Diamonds and Diamond Exploration*, J. Ross *et al.*, Eds. (Geological Society of Australia Special Publication No. 14, Perth, Australia, 1989), vol. 2, pp. 877–882.
27. S. Ono and A. Yasuda, *Phys. Earth Planet. Inter.* **96**, 171 (1996).
28. R. O. Moore and J. J. Gurney, *Nature* **318**, 553 (1985); in (*26*), pp. 1029–1041.
29. H. L. M. van Roermund and M. R. Drury, *Terra Nova* **10**, 295 (1998).
30. T. Irifune, T. Sekine, A. E. Ringwood, W. O. Hibberson, *Earth Planet. Sci. Lett.* **77**, 245 (1986); S. E. Kesson and A. E. Ringwood, *Chem. Geol.* **78**, 83 (1989); A. E. Ringwood, S. E. Kesson, W. Hibberson, N. Ware, *Earth Planet. Sci. Lett.* **113**, 521 (1992).
31. M. Akaogi and S. Akimoto, *Phys. Earth Planet. Inter.* **15**, 90 (1977).
32. ———, *Phys. Earth Planet. Inter.* **19**, 31 (1979); D. Canil, *Phys. Earth Planet. Inter.* **86**, 25 (1994).
33. T. Irifune, T. Koizumi, J. I. Ando, *Phys. Earth Planet. Inter.* **96**, 147 (1996).

34. T. Irifune and A. E. Ringwood, *Earth Planet. Sci. Lett.* **117**, 101 (1993).
35. S. E. Kesson and A. E. Ringwood, *Chem. Geol.* **78**, 97 (1989).
36. S. Heinemann, T. G. Sharp, F. Seifert, D. C. Rubie, *Phys. Chem. Miner.* **24**, 206 (1997).
37. T. Kato, A. E. Ringwood, T. Irifune, *Earth Planet. Sci. Lett.* **89**, 123 (1988).
38. M. Akaogi, Y. Hamada, T. Suzuki, M. Kobayashi, M. Okada, *Phys. Earth Planet. Inter.* **115**, 67 (1999); T. Irifune, *Nature* **370**, 131 (1994); L.-G. Liu, *Earth Planet. Sci. Lett.* **36**, 237 (1977).
39. A. E. Ringwood and J. F. Lovering, *Earth Planet. Sci. Lett.* **7**, 371 (1970).
40. W. A. Bassett and G. E. Brown Jr., *Annu. Rev. Earth Planet. Sci.* **18**, 387 (1990).
41. The infrared reflectance measurements were conducted using a Bruker IFS-66v interferometer with attached microscope; the apparatus was equipped with a globar source, KBr beamsplitter and liquid-nitrogen cooled mid-range MCT (mercury-cadmium-telluride) detector. Spectra are reported with a resolution of 4 cm^{-1} and were collected from spot sizes ranging between 40 and 90 μm in diameter; typical collection times were 3 to 10 min. Spectra reported are representative examples taken from zones of differing chemistries within the thin sections.
42. K. Omori, *Am. Mineral.* **56**, 1607 (1971).
43. M. Madon and G. D. Price, *J. Geophys. Res.* **94**, 15687 (1989).
44. J. W. Salisbury, L. S. Walter, N. Vergo, D. M. D'Aria, *Infrared (2.1-25 Micron) Spectra of Minerals* (Johns Hopkins Univ. Press, Baltimore, MD, 1991).
45. T. G. Sharp, C. M. Lingemann, C. Dupas, D. Stoffler, *Science* **277**, 352 (1997).
46. D. J. Durben and G. H. Wolf, *Am. Mineral.* **77**, 890 (1992); E. Knittle and R. Jeanloz, in *High Pressure Research in Mineral Physics*, M. H. Manghnani and Y. Syono, Eds. (American Geophysical Union, Washington, DC, 1987), pp. 243–250.
47. J. R. Brucato, L. Colangeli, V. Mennella, P. Palumbo, E. Bussoletti, *Astron. Astrophys.* **348**, 1012 (1999).
48. Geobarometers were obtained by linear regressions of pressure versus composition data (Fig. 6A) from experiments by (*32, 37, 57*). Aware of the possible effect of bulk composition on the barometers, data for garnets used for the barometer ranged from 2 to 11.13 wt% FeO: namely, 8.04 to 11.13 wt% and 6.2 to 6.4 wt% (*32*); 2.0 to 3.2 wt% (*37*); 6.09 to 6.92 wt%; and 3.7 to 6.52 wt% (*57*). This range is similar to that of the Malaita garnet: namely, 2.6 to 15.4 wt% FeO. An independent check with majorite containing 3.12 wt% FeO (*58*) from experiments at 10 GPa yields *P* estimates of 9.37 and 9.74 GPa by the Si and Al+Cr barometers, respectively.
49. A. Suzuki, E. Ohtani, T. Kato, *Science* **269**, 216 (1995).
50. S. E. Haggerty, *Earth Planet. Sci. Lett.* **122**, 57 (1994).
51. P. H. Nixon and R. H. Mitchell, *Mineral. Mag.* **43**, 587 (1980).
52. C. R. Neal and P. H. Nixon, *Trans. Geol. Soc. S. Afr.* **88**, 347 (1985); C. R. Neal, *J. Petrol.* **29**, 149 (1988).
53. H. Tsai, H. O. A. Meyer, J. Moreau, H. J. Milledge, *Mineral Inclusions in Diamond: Premier, Jagersfontein and Finsch Kimberlites, South Africa, and Williamson Mine, Tanzania*, 2nd International Kimberlite Conference, October 1977, Sante Fe, NM, F. R. Boyd and H. O. A. Meyer, Eds. (American Geophysical Union, Washington, DC, 1979), pp. 16–26.
54. A. M. Dziewonski and D. L. Anderson, *Phys. Earth Planet. Inter.* **25**, 297 (1981).
55. S. P. Grand and D. V. Helmberger, *Geophys. J. R. Astron. Soc.* **76**, 399 (1984).
56. F. J. Simmons, A. R. Zielhuis, R. van der Hilst, *Lithos* **48**, 17 (1999).
57. C. Herzberg and J. Z. Zhang, *J. Geophys. Res.* **101**, 8271 (1996); M. J. Walter, *J. Petrol.* **39**, 29 (1998).
58. S. E. Kesson, A. E. Ringwood, W. O. Hibberson, *Earth Planet. Sci. Lett.* **121**, 261 (1994).
59. R. O. Moore, M. L. Otter, R. S. Rickard, J. W. Harris, J. J. Gurney, *Geol. Soc. Aust. Abstr.* **16**, 409 (1986); T. Stachel and J. W. Harris, *Contrib. Mineral. Petrol.* **127**, 336 (1997); T. Stachel, J. W. Harris, G. P. Brey, *Contrib. Mineral. Petrol.* **132**, 34 (1998); M. L. Otter and J. J. Gurney, *Geol. Soc. Aust. Spec. Publ.* **14**, 1042 (1989); N. V. Sobolev *et al.*, *Russ. Geol. Geophys.* **38**, 379 (1997).
60. Back-scattered electron (BSE) and secondary electron (SE) images were obtained at the CMM at The University of Queensland by JEOL Super Probe and JEOL 6400F field emission scanning electron microscope, respectively.
61. A. M. Hofmeister, T. J. Fagan, K. M. Campbell, R. B. Schall, *Am. Mineral.* **81**, 418 (1996).
62. We thank A. Ewart, Y. Niu, S. Kesson, and H. O'Neil for helpful comments during the course of the research and preparation of the manuscript. We also thank J. Nailon from the CMM at The University of Queensland for patience and help during acquisition of the SEM images. P. Fredricks of the CIDC at Queensland University of Technology kindly provided the Raman spectroscopic confirmation of carbon in Fig. 4A. The manuscript was substantially improved with helpful reviews by H. Green and two anonymous reviewers. The paper is published with permission of the Directors of Solsearch Ltd.

14 February 2000; accepted 2 March 2000

Molecular Computation by DNA Hairpin Formation

Kensaku Sakamoto,[1]* Hidetaka Gouzu,[1] Ken Komiya,[1] Daisuke Kiga,[1]† Shigeyuki Yokoyama,[1] Takashi Yokomori,[3] Masami Hagiya[2]*

Hairpin formation by single-stranded DNA molecules was exploited in a DNA-based computation in order to explore the feasibility of autonomous molecular computing. An instance of the satisfiability problem, a famous hard combinatorial problem, was solved by using molecular biology techniques. The satisfiability of a given Boolean formula was examined autonomously, on the basis of hairpin formation by the molecules that represent the formula. This computation algorithm can test several clauses in the given formula simultaneously, which could reduce the number of laboratory steps required for computation.

In 1994, Adleman experimentally demonstrated that DNA molecules and common molecular biology techniques could be used to solve hard combinatorial problems (*1*), especially problems involving large searches. The data carried on a number of molecules are processed simultaneously by such techniques, and highly data-parallel computation is achieved.

Adleman's work was later generalized by Lipton (*2*), whose study encouraged further experimental work, based on Adleman and Lipton's paradigm (*3–8*). A number of theoretical studies have also emerged in the past 5 years (*9, 10*), including the idea of autonomous DNA computers (*11–14*). In these systems, the logic of computation is implemented without external control or interference (other than the regulation of temperature), which could drastically reduce the number of required laboratory steps. It has been claimed that the self-assembly and the potential to form secondary structures of the molecules are useful for the embodiment of such computers (*15–18*), but no actual computation of a hard combinatorial problem had been performed in the autonomous manner. Here, we describe a DNA-based solution of the satisfiability (SAT) problem, where the main logic of computation was implemented on the basis of hairpin formation by single-stranded DNA (ssDNA) molecules.

The SAT problem is to find Boolean-value assignments that satisfy the given formula. Each variable is assigned the Boolean value (either 0 or 1); a set of the values (a value assignment) for the variables satisfies the formula if the value of the formula becomes 1. In a subclass of the SAT problem, called conjunctive normal form (CNF)–SAT, Boolean formulas are restricted to the form of $C_1 \wedge C_2 \wedge \ldots \wedge C_n$, where each C_i is a "clause" and "$\wedge$" is the logical AND operation. A clause is of the form $L_1 \vee L_2 \vee \ldots \vee L_m$, where each L_j is a "literal" and "$\vee$" is the logical OR operation; a literal is either a variable or its negation (if variable x takes 1 or 0, then its negation, denoted by $\neg x$, takes 0 or 1, respectively).

Lipton proposed a DNA-based solution of CNF-SAT (*2*), which has been demonstrated in experimental studies (*5–8*). We took a different approach, because autonomous com-

---

[1]Department of Biophysics and Biochemistry, [2]Department of Information Science, Graduate School of Science, University of Tokyo, 7-3-1 Hongo, Bunkyo-ku, Tokyo 113-0033, Japan. [3]Department of Mathematics, School of Education, Waseda University, 1-6-1 Nishi-waseda, Shinjuku-ku, Tokyo 169-8050, Japan.

*To whom correspondence should be addressed.

†Present address: Yokoyama Cytologic Project, Exploratory Research for Advanced Technology, Japan Science and Technology Corporation, c/o RIKEN, Hirosawa, Wako-shi, Saitama 351-0198, Japan.